Science of the Total Environment 955 (2024) 176568

Contents lists available at ScienceDirect

Science of the Total Environment

journal homepage: www.elsevier.com/locate/scitotenv

In-field carbon dioxide removal via weathering of crushed basalt applied to acidic tropical agricultural soil

Fredrick J. Holden [a,b,*], Kalu Davies [a,b], Michael I. Bird [a,b], Ruby Hume [c], Hannah Green [d], David J. Beerling [b], Paul N. Nelson [a,b]

[a] College of Science and Engineering, James Cook University, Cairns, Australia
[b] Leverhulme Centre for Climate Change Mitigation, University of Sheffield, Sheffield, United Kingdom
[c] Department for Environment and Water, Adelaide, Australia
[d] College of Science and Engineering, James Cook University, Townsville, Australia

HIGHLIGHTS

- Field experiment over 5 years with basalt applied at zero or 50 t ha^{-1} a^{-1}.
- Effects of basalt weathering on soil and drainage flux chemistry quantified.
- Actual carbon dioxide capture low in tropical sugarcane system with acidic soil.
- Weathering of applied basalt was largely due to inherent (reserve) soil acidity.
- Nitric and other acids also contributed more to weathering than carbonic acid.

GRAPHICAL ABSTRACT

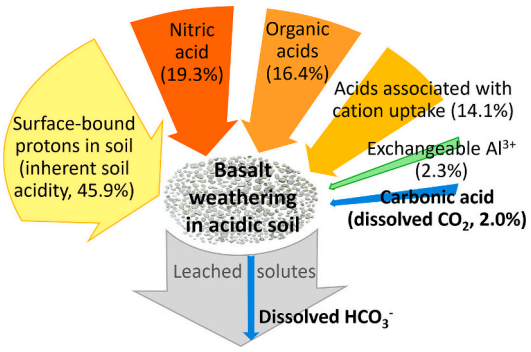

ARTICLE INFO

Editor: Shuzhen Zhang

Keywords:
Australia
Carbon capture
Climate change
Enhanced weathering
Negative emission technology
Sugarcane

ABSTRACT

Enhanced weathering (EW) of silicate rocks such as basalt provides a potential carbon dioxide removal (CDR) technology for combatting climate change. Modelling and mesocosm studies suggest significant CDR via EW but there are few field studies. This study aimed to directly measure in-field CDR via EW of basalt applied to sugarcane on acidic (pH 5.8, 0–0.25 m) Ultisol in tropical northeastern Australia, where weathering potential is high. Coarsely crushed basalt produced as a byproduct of gravel manufacture (<5 mm) was applied annually from 2018 to 2022 at 0 or 50 t ha^{-1} a^{-1}, incorporated into the soil in 2018 but not in subsequent years. Measurements in 2022 show increased soil pH and extractable Mg and Si at 0–0.25 m depth, indicating significant weathering of the basalt, but showed no increase in crop yield. Soil inorganic carbon content and bicarbonate (HCO_3^-) flux to deep drainage (1.25 m depth) were measured to quantify CDR in the 2022–2023 wet season (i.e. one year). Soil inorganic carbon was below detection limits. Mean HCO_3^- flux was 3.15 kmol ha^{-1} a^{-1} (±0.40) in the basalt-treated plots and 2.56 kmol ha^{-1} a^{-1} (±0.18) in the untreated plots but the difference (0.59 kmol ha^{-1} a^{-1} or 0.026 t CO_2 ha^{-1} a^{-1}) was not significant ($p = 0.082$). Most weathering of the basalt was attributed to acids stronger than carbonic acid. These were, in decreasing order of contribution, surface-bound protons

* Corresponding author at: College of Science and Engineering, James Cook University, Cairns, Australia.
E-mail address: fredrick.holden@jcu.edu.au (F.J. Holden).

https://doi.org/10.1016/j.scitotenv.2024.176568
Received 22 July 2024; Received in revised form 25 September 2024; Accepted 26 September 2024
Available online 9 October 2024

(inherent soil acidity), nitric acid (from nitrification), organic acids, and acids associated with cation uptake by plants. These results indicate in-field CDR via EW of basalt is low where soil and regolith pH is well below the pK_{a1} of 6.4 for H_2CO_3. However, increased soil pH, and the consumption of strong acids by weathering will eventually lead to reduced CO_2 emission from soil or evasion from rivers, with continued basalt addition.

1. Introduction

To limit global warming in the coming decades, emissions of greenhouse gases must be drastically reduced, and carbon dioxide (CO_2) removed from the atmosphere at scale (Gasser et al., 2015; Riahi et al., 2022). A promising negative emission technology is CO_2 removal via enhanced weathering of silicate rocks (Beerling et al., 2018; Hartmann et al., 2013; Köhler et al., 2010; Schuiling and Krijgsman, 2006). During weathering in suitable conditions, dissolved CO_2 or carbonic acid (H_2CO_3) reacts with silicate minerals, generating bicarbonate (HCO_3^-), other solutes, and secondary minerals such as oxyhydroxides of Fe and Al, and aluminosilicates. Taking forsterite as a simple example of a silicate, the carbonic acid weathering reaction can be represented by the equation

$$Mg_2SiO_4 + 4H_2CO_3 \rightarrow 4HCO_3^- + 2Mg^{2+} + H_4SiO_4 \quad (1)$$

in which one mole of HCO_3^- is produced per mole of non-acid cation (i.e. Ca^{2+}, Mg^{2+}, K^+, Na^+) charge in the silicate. The HCO_3^- can precipitate and accumulate in the soil as carbonates (CO_3^{2-}) or leach through the soil and travel via groundwater and rivers to the sea, where it is stored long-term as HCO_3^- and CO_3^{2-} (Berner et al., 1983). To accelerate this process, EW involves mining and crushing readily available, weatherable, non-acid-cation-rich silicate rocks such as basalt and placing them in an environment conducive to weathering such as topsoil, ideally with high pCO_2, water content, leaching and temperature, and short transport distance (Hartmann et al., 2013). Carbon sequestration, i.e. durable or permanent storage, will occur if the generated HCO_3^- and CO_3^{2-} accumulate in a highly buffered neutral-alkaline environment such as neutral-alkaline subsoils or the ocean. In addition to sequestering carbon in inorganic forms, EW could help ameliorate ocean acidification and increase carbon fixation by oceanic diatoms, which is limited by dissolved Si supply (Beerling et al., 2018; Hartmann et al., 2013). Furthermore, EW may lead to increased storage of carbon in terrestrial plant biomass (whether crops, forest or other vegetation) through augmenting the supply of limiting nutrients and ameliorating soil pH (Beerling et al., 2018; Calabrese et al., 2022; Crusciol et al., 2022; Goll et al., 2021; Hartmann et al., 2013; Kantola et al., 2023; Swoboda et al., 2022; Taylor et al., 2021; van Straaten, 2006). Similarly, EW may increase carbon storage in soil organic matter through increased inputs resulting from increased net primary production, and decreased mineralisation loss due to formation of protective secondary minerals (Buss et al., 2023; Calabrese et al., 2022; Xu et al., 2024). However, increasing the pH of acidic soils can accelerate mineralisation of soil organic matter, and some negative effects of enhanced weathering on soil organic carbon have been observed in field trials and modelling (Klemme et al., 2022; Sokol et al., 2024). The raised soil pH can reduce N_2O emissions (Blanc-Betes et al., 2021; Chiaravalloti et al., 2023) because the reduction of N_2O to N_2 is limited at pH <6.8 (Hénault et al., 2019).

Modelling indicates that EW could play a significant role in carbon dioxide removal (CDR), thereby helping mitigate anthropogenic climate change. Deployed across around half the croplands of twelve nations worldwide, EW could result in atmospheric CDR of 0.5–2.9 Pg CO_2 a^{-1} (Beerling et al., 2020; Baek et al., 2023). Life cycle assessment indicates net benefits if renewable energy is used for mining, crushing, transport and spreading and if the transport distance is not too great (Beerling et al., 2020; Lefebvre et al., 2019; Kantzas et al., 2022). Potential accumulation of toxic trace elements in the soil should also be considered (Dupla et al., 2023), but the risks will be low under normal soil conditions, as solubility and availability to plants is low even in soils developed entirely from ultramafic minerals (Chaney, 2019). Trace metals released during basalt weathering are likely incorporated into newly formed secondary minerals (Linke et al., 2024). Rates of CDR will depend on properties of the amendments, environmental conditions and application methods, and uncertainty exists around EW processes in the field (Calabrese et al., 2022; Cipolla et al., 2022; Goll et al., 2021; Larkin et al., 2022), so field experiments are crucial.

Significant weathering of crushed silicate rocks applied to soil has been measured in mesocosm and field experiments, but there have been limited measurements of CDR via EW in the field. In a field experiment in Illinois, USA, Kantola et al. (2023) estimated an average CDR of 8.6 t CO_2 ha^{-1} a^{-1} in *Miscanthus* and 3.7 t CO_2 ha^{-1} a^{-1} in maize/soybean over a 4-year period following basalt application of 50 t ha^{-1} a^{-1} and incorporation into the soil by chisel ploughing, using cation loss from the applied basalt feedstock to estimate a time-integrated CDR value. This was supported by a similar value using alternative geochemical techniques to determine dissolution rates, which gave a time-integrated potential CDR of ~2.6 t CO_2 ha^{-1} a^{-1} (Beerling et al., 2024). A much lower surface application of wollastonite (3.4 t ha^{-1}) to a forested catchment in New Hampshire, USA led to calculated cumulative CDR over 15 years of 0.025–0.130 t CO_2 ha^{-1} measured at the catchment outlet (Taylor et al., 2021). Including effects on increased forest productivity increased net CDR to 8.5–11.5 t CO_2 ha^{-1}. In a shorter-term (<6 month) study of wollastonite application to agricultural fields (1.24–5 t ha^{-1}) in Canada, CDR rates of 0.11–0.40 t CO_2 ha^{-1} were measured by change in soil inorganic carbon (Haque et al., 2020). Similar rates of CDR (0.13–0.65 t CO_2 ha^{-1}) were estimated using cation charge balance following wollastonite application (2.5–5 t ha^{-1} over 2 years) to a rubber plantation in China (Xu et al., 2024). Application of glacial rock flour with similar non-acid cation content to basalt led to CDR of 0.728 t CO_2 ha^{-1} in the 3 years following application of 50 t ha^{-1} (Dietzen and Rosing, 2023). However, in a field trial in an oil palm plantation in Sabah, Malaysia, no detectable differences in CDR, as measured by bicarbonate and other weathering products in drainage water, were found between small catchment plots with and without basalt application (50 t ha^{-1} a^{-1} for 3 years, Larkin et al., 2022). Other field trials are currently underway in America, Europe and Australia (Low et al., 2022).

Wet, warm climates are most conducive to rapid CDR via EW (Baek et al., 2023; Calabrese et al., 2022; Edwards et al., 2017; Hartmann et al., 2013; Strefler et al., 2018; Taylor et al., 2016), so field experiments in the tropics are needed to determine the maximum realistic rates of CDR via EW. However, the soils in wet climates tend to be acidic (Zhao et al., 2019) due to a preponderance of acidifying over alkalizing processes (Sumner and Noble, 2003; Van Breemen et al., 1983). Geochemical modelling of CDR via EW in an acidic environment indicates that CDR will decrease as soil pH decreases below pH 6, to an extent that depends on soil pCO_2, in a trade-off between weathering rate and carbon-capture efficiency (Bertagni and Porporato, 2022; Dietzen and Rosing, 2023; Green et al., 2024; Hartmann et al., 2013). In acidic soils, the main pool of acidity is hydrogen bound to particle surfaces ('reserve acidity'), and acidity is maintained by processes such as leaching loss of HCO_3^-, acid exudation by roots, loss of non-acid cations via export in harvested crop and by leaching, along with accumulation of exchangeable Al^{3+}, and nitrification (Weil and Brady, 2017). In addition to surface-bound hydrogen, common soil acids include, in increasing order of strength, dissolved CO_2 or carbonic acid ($pK_{a1} = 6.4$ at 25 °C), exchangeable Al^{3+} ($pK_{a1,2} = 5.0, 5.1$), organic acids ($pK_{a1} =$

3–5) and nitric acid ($pK_{a1} = -1.3$). To address uncertainties in CDR rates via EW, the aim of this work was to directly measure in-field CDR via EW of crushed basalt (produced as a byproduct of gravel manufacture) in an acidic tropical agricultural soil. This was achieved by measuring accumulation of carbon in the soil (over 5 years), and bicarbonate fluxes from the root zone (in the 5th year), and by determining the contribution of soil acids to weathering of the applied basalt.

2. Methods

2.1. Experimental site characteristics and treatments

The experimental site is a commercial sugarcane (*Saccharum* hybrid) field near Gordonvale in Queensland, Australia (17.085° S, 145.807° E, Fig. S1) at 17–20 m elevation on a Pleistocene terrace of the Mulgrave River with a well-drained red Kandosol (Table S1), Virgil soil series (Murtha et al., 1996) or kaolinitic Udult (Soil Survey Staff, 2022). The profile is described in more detail in Table S1. A detailed survey of apparent electrical conductivity using a Geonics EM38 (one point every ~3 m) showed very uniform soil across the site. Soil $pH_{(1:5\ soil:water)}$ was initially 5.83 ± standard error of the mean (SEM) of 0.09 at 0–0.25 m depth and 5.35 ± 0.06 at 25–50 cm depth in the experimental plots in 2018. The area in which the field is situated has no natural or manmade surface drainage, with all rainfall infiltrating, and a water table deeper than approximately 5 m. Average annual rainfall is 2037 mm and mean annual temperature is 25 °C (2013–2023, Meringa Sugar Experiment Station 31040). Most rain falls in a distinct wet season between December and May. Daily rainfall during the experiment was recorded at Mulgrave Mill, 2 km from the site. Sugarcane has been grown on the site for >100 years. The typical crop cycle for sugarcane in the region is 5 annual harvests before the crop is ploughed out and replanted following a short wet-season fallow. The first year of the cycle is called the plant crop and the subsequent years are called ratoons. The studied crop (cultivar Q253) was planted in May 2018 following a wet season fallow of soybean. The experiment is a randomised block design with 4 replicates per treatment. Plots are 550 m long and 5 rows wide (8.25 m), with one guard row (1.65 m) between each plot (Fig. S1).

Crushed basalt was broadcast annually at 0 or 50 t ha^{-1} from 2018 to 2022, using a mechanical spreader with GPS- and computer-controlled rate delivery. The first basalt application was in May 2018 onto the herbicide-killed soybean fallow crop. The field rows were then cultivated using a rotary hoe (approximately 0.2 m deep) and planted to sugarcane. When the plants were established, the rows were 'hilled up'. Subsequent basalt applications, made following harvest each year, were not incorporated because no cultivation is carried out during ratoons. When basalt was spread in 2022, a 5 × 5 m area within each plot, 25 m in from the western end of the trial, was covered during the main application and then the basalt was spread by hand, to ensure even distribution. Soil and leachate (deep drainage) was sampled within this subplot. The basalt was commercial 'crusher dust' produced as a by-product of aggregate production at the Tichum Creek quarry (16.970° S, 145.5367° E) in the Atherton Basalt Province (Whitehead et al., 2007). It had been sieved through a screen at the quarry, <4 mm in 2018–2020 and < 5 mm in 2021–2022. Particle size was coarse, with 14–29 % being <1 mm and 40–60 % being <2 mm (Fig. S3). Quantitative mineralogy was determined with XRD, aided by observations made through SEM-EDS analysis. It gave a composition of augite (42.3 %), olivine (19.4 %), leucite (13.4 %), plagioclase (10.4 %), analcime (5.8 %), basaltic glass (2.6 %), orthoclase (2.4 %), apatite (2 %) and ilmenite (1.9 %), with a low content of calcite (0.2 %) (Lewis et al., 2021), but considerably more glass was observed in some samples. It has relatively low Si content 42–46 % SiO_2, Table S2). The BET specific surface area of the basalt applied in 2018 is 10.3 $m^2\ g^{-1}$ (Lewis et al., 2021). Mineralogy of the basalt varied little between batches (Table S3). Based on its non-acid cation content (6.3 % Ca, 2.8 % Mg, 0.9 % K and 3.2 % Na) and a carbonic weathering reaction that converts one mole of CO_2 to HCO_3^- per mole of non-acid cation charge (Eq. (1), Hartmann et al., 2013), the potential mass of CO_2 converted per mass of basalt, or R_{CO2}, is 0.31.

Agronomic management at the trial site followed normal farming practices, except that lime was not applied prior to planting of the sugarcane, to measure the liming effect of basalt alone. Fertiliser was applied as granular blends in a band drilled by coulters into the centre of the row (~100 mm depth) at recommended rates (Calcino et al., 2018), with the plant crop receiving 130 kg N ha^{-1} (as urea, diammonium phosphate and ammonium sulfate), 94 kg K ha^{-1} (as potassium chloride), 60 kg S ha^{-1} (as ammonium sulfate), 10 kg P ha^{-1} (as diammonium phosphate) and 6 kg Zn ha^{-1} (as zinc sulfate monohydrate) and the ratoon crops receiving 125–148 kg N ha^{-1} (mostly as urea) 90–107 kg K ha^{-1} (as potassium chloride) and 0–15 kg S ha^{-1} (as ammonium sulfate) per year, 'stool-split' approximately 3–4 weeks after harvest, and all rates being expressed on an annual basis. The same fertiliser regime was in place for 10 years prior to the start of the trial, except for N rates, which may have been slightly higher ~160 kg ha^{-1} from 10 to 5 years prior to the start of the trial. Before that, P rates were considerably higher although records are not available.

2.2. Sugarcane and soil sampling and analysis

Sugarcane yield was measured from all 5 rows and cane and leaf samples were taken from the central 3 rows. The sugarcane is mechanically harvested 'green' (without prior burning), so at each harvest a layer of leaves rejected by the harvester ('trash', ~5 t dry matter ha^{-1}) was deposited on top of the previous basalt application. Cane yield (fresh weight) and sugar content (commercial cane sugar, CCS) were measured annually at the Mulgrave sugar mill. Subsamples of cane (which is removed permanently from the field) and leaves (returned to the field) taken at harvest were analysed for contents of N, P, K, Ca, Mg, Na, S, B, Cu, Fe, Mn, Zn, Mo and Si.

Soil was sampled and analysed following harvest in October 2022. Samples were taken at 0–0.10, 0.10–0.25 and 0.25–0.50 m depths (composite of 6 points across the central row and adjacent interrow). Samples were analysed (with codes for methods from Rayment and Lyons, 2011) for $pH_{1:5\ soil:water}$ (4A1), electrical conductivity ($EC_{1:5}$, 3A1), exchangeable non-acid cations (1 M ammonium acetate, 15D3), exchangeable acidity (1 M KCl, 15G1), extractable P and Si (0.005 M H_2SO_4, 9G2), and total C and N (dry combustion, 6B2b, 7A5) by the Nutrient Advantage laboratory, Werribee, Australia. Soil pore water composition, in particular pH, is critical for weathering, and $pH_{1:5\ soil:water}$ closely mimics pore water pH in tropical soils (Bruce et al., 1989). Air drying prior to analysis may have resulted in exchangeable Al^{3+} being slightly underestimated and pH slightly over-estimated (Gillman and Murtha, 1983). Inorganic C was measured by using a pressure-calcimeter (Sherrod et al., 2002). Extractable alkalinity was measured by titration of a 1:1 soil:solution (0.01 M $CaCl_2$) extract. Soil bulk density and pH buffering capacity were measured in samples taken in 2020 and 2021. Bulk density was measured in 0.2 m increments to 1.2 m (50-mm diameter core). Soil pH buffering capacity was measured using a method adapted from Wang et al. (2015, 2017). The alkali solution added was composed to mimic the ionic composition of the Tichum basalt (molar Mg:Ca:Na ratio of 0.443:0.325:0.232), using 0.2 M $NaHCO_3$ solution added to a background solution of 0.01 M $MgCl_2$/$CaCl_2$ (0.577:0.423 M ratio).

2.3. Leachate sampling and analysis

In November 2022, two passive-wick drainage flux meters (DFMs, Tranzflo NZ Ltd.) (Gee et al., 2009) of 0.2 m diameter were installed in each plot, one beneath the row (R), and one beneath the interrow (IR). The DFMs collected leachate at 1.25 m beneath the ground surface and tubes to the surface allowed leachate removal (Fig. S2). Excavated soil was replaced in layers to the original bulk density and sugarcane plants

were replaced above the DFMs. During earlier wet seasons, collection of leachate was attempted using ceramic suction cup lysimeters but it was often not possible to obtain samples, and insufficient data was collected to confidently test treatment effects.

During the 2022–2023 hydrological year (i.e. 1 December 2022 to 30 November 2023) all the leachate reaching the DFMs as deep drainage was collected and analysed. This was in 25 sampling events, each within 1–2 days following significant rainfall events, allowing sufficient time for drainage. Collected volume was measured in-field and samples were placed into HDPE bottles with no headspace, cooled and taken to the laboratory where they were returned to room temperature and analysed for pH, EC and alkalinity (Hach AT1000 autotitrator) within 24 h. Proton concentrations were calculated from pH and used to determine mean pH values and proton fluxes. Samples from all DFMs in 8 drainage events distributed evenly through the period of leaching (27/12/2023, 3/1/2023, 17/1/2023, 31/1/2023, 20/2/2023, 7/3/2023, 30/3/2023, 26/4/2023) were stored frozen and analysed for anion concentrations (nitrate, nitrite, sulfate, chloride, phosphate) using ion chromatography (Metrohm 930 Compact IC Flex ion chromatograph, with a Metrosep A Supp 5–100/4.0 column) calibrated with commercial standards (Merck). Concentrations of nitrite and phosphate were negligible and are not reported. The concentration of organic anions was calculated as the difference between total ionic strength and the sum of measured anion concentrations, with total ionic strength (I, $mmol_c\ L^{-1}$) calculated from EC ($\mu S\ cm^{-1}$) using the eq. $I = (12*EC/1000) - 0.4$ (Gillman and Bell, 1978). Concentrations of nitrate (NO_3^-), chloride (Cl^-) and organic anions (OA) in the unanalysed samples were estimated from EC using regressions developed from the 8 events for which all analyses were conducted ($p < 0.001$ and adjusted r^2 of 0.731, 0.823 and 0.853, respectively). Sulfate concentration was not significantly related to EC but was significantly related to individual DFMs ($p = 0.002$) so the mean of analysed values for each DFM was used as the estimate for unanalysed samples. Reported alkalinity was converted into HCO_3^- concentration, assuming all alkalinity was HCO_3^-, due to the pH, temperature, and pressure of the water. Cumulative flux of solutes below the root zone was calculated for each DFM by multiplying concentration by volume for each drainage event and summing the amounts. CDR via EW was calculated as the difference in cumulative leached HCO_3^- between the basalt-treated and untreated plots.

2.4. Measuring the contribution of strong acids to basalt weathering

The contribution of soil acids to weathering of the applied basalt was determined by measuring the impact of the acid-base reactions involved. For carbonic acid, that was the generation of HCO_3^-, as described above. The reaction of surface-bound protons in variably charged minerals and organic matter with alkali was quantified by the change in soil pH over the course of the experiment, together with soil pH buffering capacity and bulk density, as variable charge accounts for >90 % of the pH buffering in acidic tropical soils (Nelson and Su, 2010; Weil and Brady, 2017). The reaction of soil exchangeable Al^{3+} with alkalinity was quantified by the decrease in exchangeable Al^{3+} in the 0–0.25 m increment over the 4-year period, assuming 2 mol of H^+ per 3 $mole_c$ of Al^{3+}. Acidification associated with cation uptake was quantified by summing the cations in the sugarcane stalks and leaves at harvest and taking the difference between the plots with and without applied basalt. These cations may have been taken up together with the anions generated during the weathering, or their uptake may have been balanced by exudation of protons; either way, they are associated with soil acidification. This estimate of acidification based on cation uptake is conservative as it does not include the acidifying effect of ammonium uptake, which sugarcane is known to prefer over nitrate (Robinson et al., 2011). The reaction of organic acids exuded by roots and microorganisms with alkali was estimated from organic anion flux in deep drainage. This was calculated as the difference between organic anion flux in the basalt-treated and untreated plots. It may be an overestimate as it assumes exudation of organic acids in protonated form rather than as anions, although we have no reason to believe that addition of basalt would stimulate organic anion production. The reaction of nitric acid with alkali was quantified by the cumulative flux of nitrate in deep drainage, and the contribution of nitric acid to basalt weathering was calculated as the difference in nitrate flux between the basalt-treated and untreated plots. All nitrate must have originated from nitric acid generated by nitrification, as no nitrate was added. Nitrification produces either 1 mol of H^+ per mole nitrogen if it originates from urea or mineralisation of organic N, or 2 mol of H^+ per mole of nitrogen if it originates from NH_4^+. We assumed the former, as 96 % of fertiliser N applied in 2022 was in the form of urea and only 4 % in the form of NH_4^+.

2.5. Statistical analyses

The effect of the treatments on soil properties, yield, and cumulative leaching of HCO_3^- and other anions, was analysed by one-way analysis of variance (ANOVA) using R (v4.4.0; R Core Team, 2024) in RStudio (v2024.4.0.735; Posit team, 2024). For the cumulative leaching data, results for row and inter-row samples were averaged for each plot, giving 4 replicate values per treatment, one for each plot. Results were also analysed with a split-plot design, in which the main plot was basalt and the split-plot was location (row versus inter-row). In cases where location was significant, results of the split-plot ANOVA are presented and in cases where location was not significant results of the one-way ANOVA are presented. For the solute concentration data, time of sampling was an additional effect. For that data, generalised linear mixed effect modelling (GLMM) using the glmmTMB R package (v1.1.9; Brooks et al., 2017) was used to determine the effects of basalt and location as factors, including time as a random effect. In all statistical analyses the data were checked for normality and other assumptions using DHARMa R package and simulateResiduals function (v0.4.6; Hartig, 2022), and transformations (log, Box Cox or inverse) were applied where necessary. Generalised additive models (GAM) with fixed effects using the mgcv R package and gam function (v1.9.1; Wood, 2011) were used to illustrate the time course of cumulative HCO_3^- leaching flux, and leachate pH and HCO_3^- concentration. The effect of location (row versus interrow) on pH and HCO_3^- concentration was also tested in the GAM analysis but it did not improve model quality according to the Aikake information criterion so it is not reported.

3. Results

3.1. Basalt effects on soil, crop and leachate

Despite its coarse particle size, significant weathering of the applied basalt occurred by 2022 after 5 applications, as indicated by an increase in soil pH, exchangeable Mg and Na to 0.25 m depth and extractable Si to 0.5 m depth over the course of the trial (Table 1). Mean exchangeable Al decreased near the surface but the effect was not significant ($p = 0.095$ at 0–0.1 m). There was no significant change in soil total C content ($p > 0.1$ at all depths), and total inorganic C and extractable inorganic C contents were below detection limits (<0.3 g kg^{-1} and < 0.05 mmol kg^{-1}, respectively) for all samples, as expected at this soil pH. Despite the improved soil conditions, including higher pH and availability of Mg and Si, there was no significant ($p < 0.05$) effect of the basalt treatment on cane yield, sugar or nutrient contents of the cane or leaves (Table S1). In 2022 the mean cane yield across all plots was 81 t ha^{-1} and mean sugar content was 13.3 % CCS. There were slight increases in leaf contents of Mg (0.10 to 0.13 %, $p = 0.095$), K (1.09 to 1.30 %, $p = 0.089$), Cu (2.15 to 2.75 mg kg^{-1}, $p = 0.064$) and Zn (15.8 to 20.8 mg kg^{-1}, $p = 0.086$), and slight decreases in cane contents of N (0.21 to 0.15 %, $p = 0.051$), Ca (0.04 to 0.03 %, $p = 0.090$) and Mn (79.5 to 63.5 mg kg^{-1}, $p = 0.077$) (Table S4).

Leachate pH and the concentrations of HCO_3^- and other solutes in leachate were not significantly affected by basalt application (Table 2).

Table 1
Effect of basalt application on selected soil properties in 2022, following 4 years of treatment. $n = 4$ (each being a composite). SEM = standard error of the mean. Variables with $p < 0.05$ from the one-way ANOVA are shown in bold.

	No basalt		Basalt		p
	Mean	(SEM)	Mean	(SEM)	
0–0.1 m depth					
$pH_{(1:5\ soil:water)}$	**5.63**	**(0.11)**	**6.13**	**(0.05)**	**0.006**
Total C (g kg^{-1})	10.00	(0.64)	10.08	(0.72)	0.941
Total N (g kg^{-1})	0.65	(0.05)	0.72	(0.06)	0.442
CEC ($cmol_c$ kg^{-1})	1.86	(0.24)	2.21	(0.11)	0.231
Exch. Al ($cmol_c$ kg^{-1})	0.44	(0.11)	0.25	(0.03)	0.095
Exch. Ca ($cmol_c$ kg^{-1})	0.97	(0.25)	1.10	(0.11)	0.640
Exch. K ($cmol_c$ kg^{-1})	0.22	(0.02)	0.26	(0.02)	0.227
Exch. Mg ($cmol_c$ kg^{-1})	**0.24**	**(0.06)**	**0.54**	**(0.03)**	**0.005**
Exch. Na ($cmol_c$ kg^{-1})	**0.01**	**(0.00)**	**0.07**	**(0.01)**	**<0.001**
Extr. P (mg kg^{-1})	142.5	(7.5)	157.5	(7.5)	0.207
Extr. Si (mg kg^{-1})	**55.8**	**(14.9)**	**450.0**	**(131.0)**	**0.002**
0.1–0.25 m depth					
$pH_{(1:5\ soil:water)}$	5.60	(0.11)	5.85	(0.03)	0.067
Total C (g kg^{-1})	9.18	(0.36)	9.75	(0.15)	0.194
Total N (g kg^{-1})	0.63	(0.03)	0.61	(0.03)	0.700
CEC ($cmol_c$ kg^{-1})	1.84	(0.17)	1.90	(0.14)	0.773
Exch. Al ($cmol_c$ kg^{-1})	0.50	(0.10)	0.44	(0.05)	0.666
Exch. Ca ($cmol_c$ kg^{-1})	1.00	(0.21)	0.89	(0.12)	0.661
Exch. K ($cmol_c$ kg^{-1})	0.17	(0.01)	0.17	(0.01)	0.885
Exch. Mg ($cmol_c$ kg^{-1})	**0.21**	**(0.04)**	**0.33**	**(0.04)**	**0.047**
Exch. Na ($cmol_c$ kg^{-1})	**<0.02**	**(<0.02)**	**0.06**	**(0.01)**	**0.011**
Extr. P (mg kg^{-1})	147.5	(4.8)	140.0	(7.1)	0.414
Extr. Si (mg kg^{-1})	**70.5**	**(27.9)**	**232.5**	**(44.2)**	**0.021**
0.25–0.5 m depth					
$pH_{(1:5\ soil:water)}$	5.35	(0.09)	5.48	(0.05)	0.253
Total C (g kg^{-1})	7.30	(0.45)	7.43	(0.41)	0.844
Total N (g kg^{-1})	0.57	(0.04)	0.53	(0.01)	0.617
CEC ($cmol_c$ kg^{-1})	1.46	(0.10)	1.51	(0.07)	0.692
Exch. Al ($cmol_c$ kg^{-1})	0.77	(0.09)	0.79	(0.07)	0.887
Exch. Ca ($cmol_c$ kg^{-1})	0.49	(0.14)	0.41	(0.08)	0.750
Exch. K ($cmol_c$ kg^{-1})	0.11	(0.01)	0.11	(0.01)	0.815
Exch. Mg ($cmol_c$ kg^{-1})	0.12	(0.03)	0.16	(0.02)	0.142
Exch. Na ($cmol_c$ kg^{-1})	<0.02	(<0.02)	0.04	(0.01)	0.057
Extr. P (mg kg^{-1})	66.5	(12.1)	88.5	(15.6)	0.308
Extr. Si (mg kg^{-1})	**41.3**	**(12.6)**	**147.0**	**(40.4)**	**0.024**

Table. 2
Effect of basalt application on deep drainage pH and ion concentrations. For pH, HCO_3^- and EC, n = 346. For the other anions n = 96. P-values from GLMM with basalt and location as factors, and time as a random effect.

Variable	0, IR	0, R	50, IR	50, R	Basalt	Location
	Mean	Mean	Mean	Mean	p	p
pH	6.41	6.12	6.31	6.21	0.815	**0.045**
HCO_3^- (mmol L^{-1})	0.78	0.97	0.89	0.63	0.939	0.220
Cl^- (mmol L^{-1})	0.08	0.34	0.07	0.33	0.292	**<0.001**
NO_3^- (mmol L^{-1})	0.18	0.81	0.11	0.98	0.594	**<0.001**
SO_4^{2-} (mmol$_c$ L^{-1})	0.17	0.11	0.15	0.13	0.235	**<0.001**
OA (mmol$_c$ L^{-1})	0.28	2.00	0.23	1.27	0.083	**<0.001**
EC	155.8	493.6	172.1	304.2	0.094	**<0.001**

They were generally highest in the first few weeks of deep drainage, declining to low levels by January and then increasing slightly following periods of low rainfall in March (Fig. 1). Over the whole season, mean pH of the leachate was 6.27 and mean HCO_3^- concentration was 0.818 mmol L^{-1} (SEM = 0.090). Leachate pH and HCO_3^- concentrations were typically most variable in the row, in the first half of the wet season. The first leachate samples, with very small volumes, were all in the interrow, with relatively high pH and concentrations of HCO_3^-. The lowest values were reached in several DFMs in January. Mean cumulative deep drainage flux of HCO_3^- was slightly higher in basalt treatments over the course of the year (Fig. 2) but the total cumulative amount leached (annual mean of 3.15 kmol ha^{-1} with basalt and 2.56 kmol ha^{-1} without basalt) did not differ significantly between treatments (Table 3). The highest cumulative value from an individual DFM was 5.33 kmol ha^{-1} (in a plot with 50 t $ha^{-1}a^{-1}$ of basalt, in the row). The amount of CDR via EW, i.e. the difference in HCO_3^- deep drainage flux between basalt-treated and untreated plots (keeping in mind that there was no increase in soil inorganic carbon, which was not detectable in any plots), was 0.59 kmol $ha^{-1}a^{-1}$ or 0.026 t CO_2 $ha^{-1}a^{-1}$. Deep drainage flux of H^+ also did not differ significantly between treatments (Table 3). Leachate pH was lower, and concentrations and fluxes of Cl^-, NO_3^- and organic anions were all higher in the row than the interrow (Table 2 and 4).

3.2. Contribution of strong acids to weathering of basalt

Changes in soil properties and deep drainage fluxes of anions suggested that the strong acids responsible for most of the basalt weathering were surface-bound protons, nitric acid, organic acids, and acid exuded by roots to balance cation uptake (Fig. 3). The largest contributor was the inherent soil acidity associated with surface-bound protons. The measured change in soil pH at 0–0.5 m depth corresponded to consumption of 10 $kmol_c$ ha^{-1} a^{-1} of alkalinity. Assuming alkalinity consumption in the 0.5–1.25 m depth increment was half that in the 0.25–0.5 m increment, on a per soil volume basis, the total consumption of alkalinity was 13.7 $kmol_c$ ha^{-1} a^{-1} in the profile above the point of leachate collection. Nitric acid and organic acids contributed similar amounts of acidity in the row, where fertiliser (including urea and ammonium) was placed and root and microbial activity were highest. In the interrow, less nitric and organic acids were generated. Total uptake of non-acid cations (Ca, Mg, K and Na) was 4.20 $kmol_c$ ha^{-1} greater in the basalt-treated plots (mean 76.2 $kmol_c$ ha^{-1}, SEM 5.1) than the untreated plots (mean 72.0 $kmol_c$ ha^{-1}, SEM 3.7). Exchangeable Al^{3+} contributed little to weathering. Overall, an estimated total acidity of 29.8 kmol $ha^{-1}a^{-1}$ was consumed in weathering the basalt, of which 2.0 % was due to carbonic acid (Fig. 4).

4. Discussion

4.1. Carbon dioxide removal via carbonic acid weathering

The cumulative addition of 250 t ha^{-1} of coarsely crushed basalt to a sugarcane field over 5 years resulted in a statistically insignificant ($p = 0.082$) in-field CDR via EW (i.e. increase in soil carbonate plus export of bicarbonate in deep drainage) of 0.026 t CO_2 ha^{-1} a^{-1} being measured in the 5th year. This value is low compared to the potential CDR determined using measured basalt dissolution rates in a field trial in mid-west USA (10.5 ± 3.8 t CO_2 $ha^{-1}a^{-1}$) in which 200 t ha^{-1} of basalt was applied and incorporated by annual chisel ploughing over 4 years (Beerling et al., 2024). However, our results are consistent with those of Larkin et al. (2022), who found no detectable CDR via EW measured as bicarbonate in stream drainage in a field trial in Malaysia, and a small increase in soil carbonate (~0.26 t CO_2 ha^{-1} a^{-1}) that could not definitively be attributed to basalt weathering. As far as we are aware, the Malaysian study is the only other study to directly measure in-field CDR via EW in a tropical region. In a field trial in tropical China, potential CDR was estimated from cation charge balance as 0.13 and 0.65 t CO_2 ha^{-1} following 2.5 and 5.0 t ha^{-1} applications of wollastonite, respectively (Xu et al., 2024). However, there was a substantial increase in soil organic C. Across these three tropical field trials, low soil pH may have been at least partially responsible for low CDR, due to the effects of pH on carbonate equilibria. Initial soil pH was (0–0.3 m depth) 5.1 ± 0.55 at the Malaysian site (Larkin et al., 2022), around 4.9 at the Chinese site (Xu et al., 2024), and 5.8 ± 0.09 at our site. In soil, carbonic acid dissociates only at pH greater than approximately 5.5 so it will contribute little to weathering (Eq. (1)) where pH is below this value (Bertagni and Porporato, 2022; Dietzen and Rosing, 2023; Green et al., 2024;

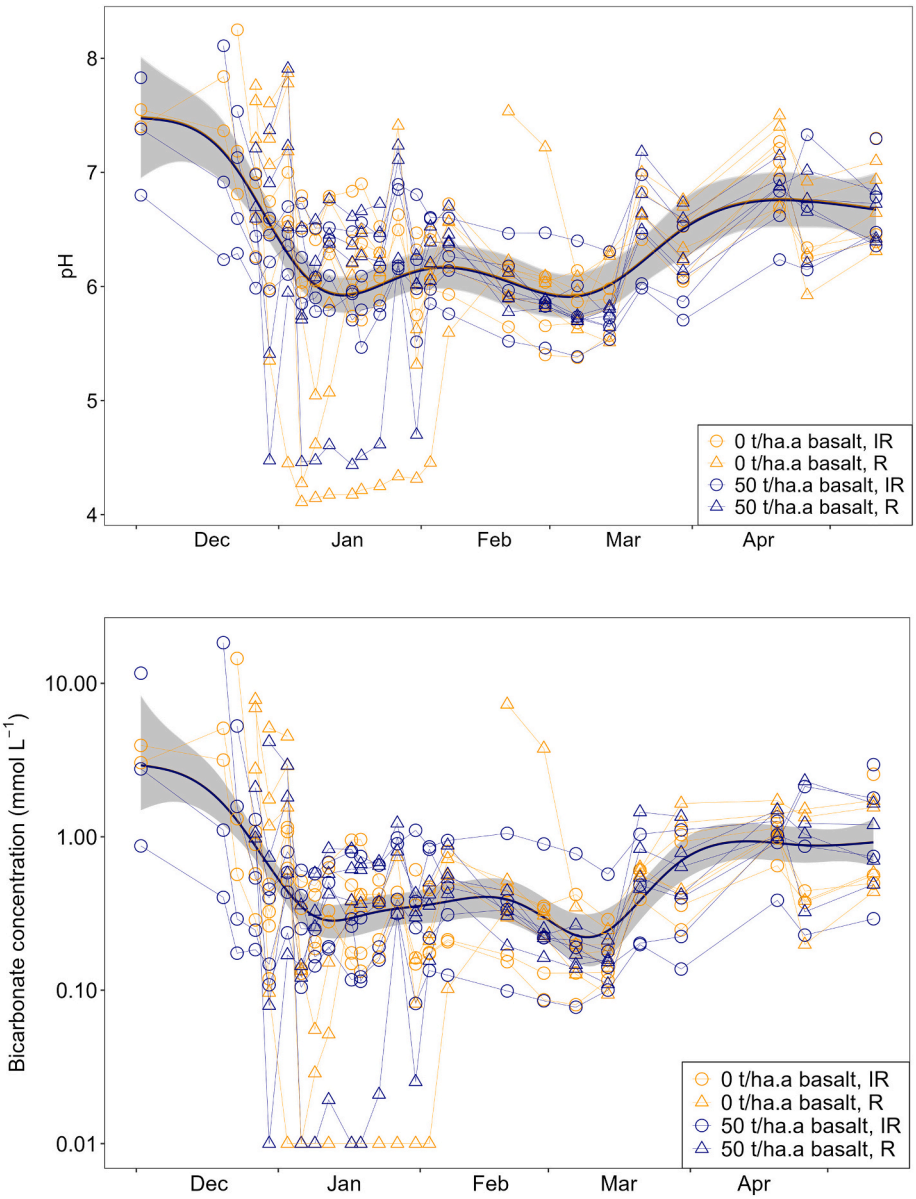

Fig. 1. pH and concentration of HCO_3^- in leachate collected as deep drainage over the 2022–2023 wet season. Each symbol and thin line represents an individual drainage flux meter. R = row and IR = Interrow. Concentrations of HCO_3^- below the detection limit are shown as 0.01 mmol L^{-1}. Results of statistical analyses are shown in Table 4. Thick lines show generalised additive models (GAMs), with the two lines (with or without basalt) and 95 % confidence intervals (grey area) overlapping completely. To meet the assumption of normality for GAM the concentration data was inverse transformed, but the results have been back-transformed to be shown on the same scale as the data.

Hartmann et al., 2013). However, it is also possible that other soil properties and land management practices in these tropical agricultural systems contributed the low or insignificant CDR values measured or estimated.

Thus, the predominant silicate weathering reaction in acidic soils such as that in our trial, taking forsterite as a simple example of a silicate and HA to represent the acids stronger than carbonic acid (with A representing the anion or negatively charged particle), must be:

$$Mg_2SiO_4 + 4HA \rightarrow 4A^- + 2Mg^{2+} + H_4SiO_4 \quad (2)$$

Carbonic acid weathering (Eq. (1)) occurred only to a small extent in our field trial but it might be expected to be the predominant weathering reaction in soil with pH around 6.4, the pK_1 of carbonic acid, depending on soil pCO_2. The main silicate minerals weathering in our field trial were augite ((Ca,Na)(Mg,Fe,Al,Ti)$(Si,Al)_2O_6$) and olivine ((Mg,Fe)$_2SiO_4$) rather than only the Mg-olivine forsterite in Eq. (2) (Lewis et al., 2021). During weathering of these minerals, Ca and Na would have behaved similarly to the Mg in Eq. (2), and Fe and Al presumably formed secondary oxyhydroxide and aluminosilicate minerals.

Eq. (2) represents a simplified summary of the reactions occurring in the soil above the point of leachate collection. However, it is probable that carbonic acid weathering (Eq. (1)) occurred in the top few centimetres, where basalt concentration and pH were highest, but that the HCO_3^- generated by this weathering was converted to CO_2 deeper in the profile, where pH was lower and there was no basalt, via the reaction

$$HCO_3^- + HA \rightarrow CO_2 + A^- + H_2O \quad (3)$$

The mean HCO_3^- export in leachate across all treatments (2.85 kmol ha^{-1} a^{-1}, a CDR of 0.125 t CO_2 ha^{-1} a^{-1}) was the same order of magnitude as HCO_3^- export in the Johnstone River (6.1 kmol ha^{-1} a^{-1}, Rosentreter and Eyre, 2019), which is nearby and experiences a similar climate. The Johnstone River catchment is dominated by basalt,

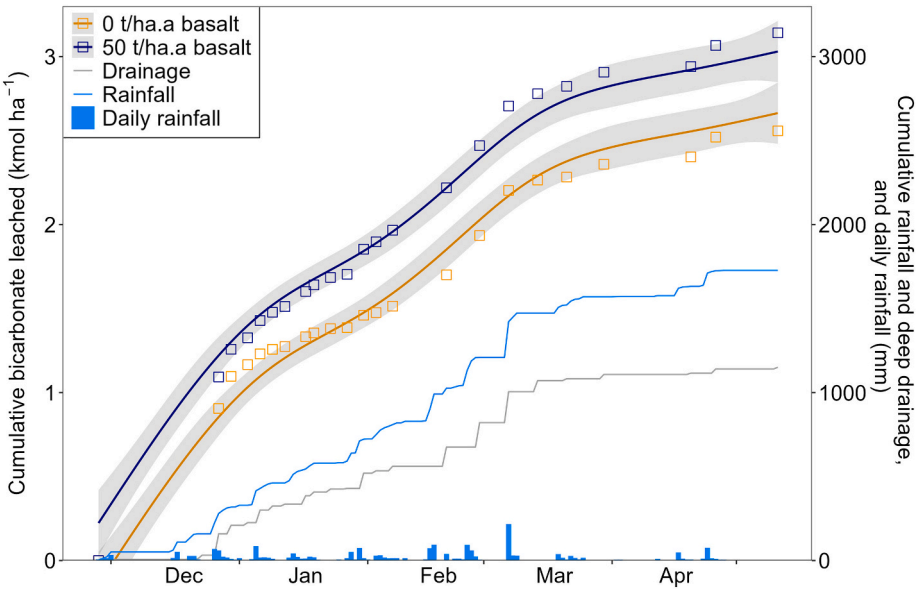

Fig. 2. Cumulative mean deep drainage flux of HCO_3^- in the two treatments (squares) and fitted GAMs, showing 95 % confidence interval (grey shading), over the 2022–2023 wet season. The earliest non-zero values represent the first time when leachate was collected in all drainage flux meters (27 December 2022); those values combine amounts for several small earlier events (starting on 2 December 2022) that did not lead to leachate in all drainage flux meters. No leachate was generated after 11 May 2023. Cumulative rainfall and drainage and daily rainfall are also shown. Results of the statistical analysis of cumulative HCO_3^- flux for the whole year are shown in Table 2.

Table 3
Effect of basalt application on cumulative ion fluxes as deep drainage in the 2022–2023 hydrological year, following 4 years of treatment. Cumulative fluxes of Cl^-, NO_3^-, SO_4^{2-} and organic anions (OA) include estimated values for the events not analysed. SEM = standard error of the mean. P-values are from one-way ANOVA.

Variable	No basalt		Basalt		p
	Mean	(SEM)	Mean	(SEM)	
H^+ (mol ha^{-1})	42.3	(36.2)	23.1	(17.0)	0.978
HCO_3^- (kmol ha^{-1})	2.56	(0.18)	3.15	(0.40)	0.082
Cl^- (kmol ha^{-1})	0.84	(0.24)	1.13	(0.25)	0.242
NO_3^- (kmol ha^{-1})	2.04	(0.63)	2.88	(0.79)	0.196
OA (kmol$_c$ ha^{-1})	3.78	(1.30)	4.88	(1.37)	0.320
SO_4^{2-} (kmol$_c$ ha^{-1})	0.81	(0.19)	1.24	(0.32)	0.148

suggesting more weatherable material than at the studied field site. However, most of the basalt is older than 2.8 Ma and the regolith is highly weathered (Whitehead et al., 2007). To put these CDR values in perspective, the highest riverine export of HCO_3^- in the global database of Dessert et al. (2003) is 64.1 kmol ha^{-1} a^{-1} (2.82 t CO_2 ha^{-1} a^{-1}) in a basaltic catchment with humid tropical climate in Java. The small amount of HCO_3^- in rivers draining highly weathered tropical landscapes has been found to be associated with non-acid cations released from biomass during decomposition in surface layers and burning, rather than from weathering of silicates (Markewitz et al., 2001). Although insignificant in-field CDR via EW was measured in the current study, there was considerable weathering of the applied basalt, as indicated by the increase in soil pH, exchangeable Mg and Na and extractible Si (Table 1), and the ratio of immobile (Ti) to mobile (Ca and Mg) elements originating from the applied basalt measured by Reershemius et al. (2023). Our results indicate this weathering was caused primarily by acids stronger than carbonic acid.

4.2. *Acids responsible for weathering of basalt*

Surface-bound protons were identified as the main acid contributing to weathering, which corresponds to their status as the main store of inherent acidity in acidic soils (Weil and Brady, 2017). It has been suggested that exchangeable acidity (Al^{3+} and H^+) would reduce EW efficiency in acidic soils (Calabrese et al., 2022), but it played only a small role in this study; the decrease in exchangeable Al^{3+} was statistically insignificant (Table 1). The consumption of reserve acidity we found in the field reflected the results of Gillman et al. (2002), who applied finely ground basalt to a range of acidic tropical soils in an incubation experiment. The effects of basalt on soil pH, exchangeable Mg and extractable Si were also similar between the two studies, but effects on CEC, exchangeable Al, Ca and K, and extractable P found by Gillman et al. (2002) were not reflected significantly in our field study. Nitrogen fertiliser, and the subsequent transformations and movement of nitrogen, had a large effect on weathering and leachate composition. Nitrification is responsible for much of the acidification in agricultural systems (Bolan and Hedley, 2003) and the effect on CDR that we measured has been predicted (Hartmann et al., 2013). The well-drained

Table 4
Means and *p* values for leachate fluxes that were significantly ($p < 0.05$) affected by location (i.e. row, R, versus interrow, IR). 0 = no basalt, 50 = basalt at 50 t ha^{-1} a^{-1}. P-values are from split-plot ANOVA.

Variable	0, IR	0, R	50, IR	50, R	Basalt	Location	Bas.*Loc.
	Mean	Mean	Mean	Mean	p	p	p
Cl^- (kmol$_c$ ha^{-1})	0.47	1.22	0.59	1.67	0.179	**0.007**	0.596
NO_3^- (kmol$_c$ ha^{-1})	1.04	3.05	1.10	4.65	0.099	**0.002**	0.346
OA (kmol$_c$ ha^{-1})	1.66	5.89	1.79	7.97	0.174	**0.002**	0.532

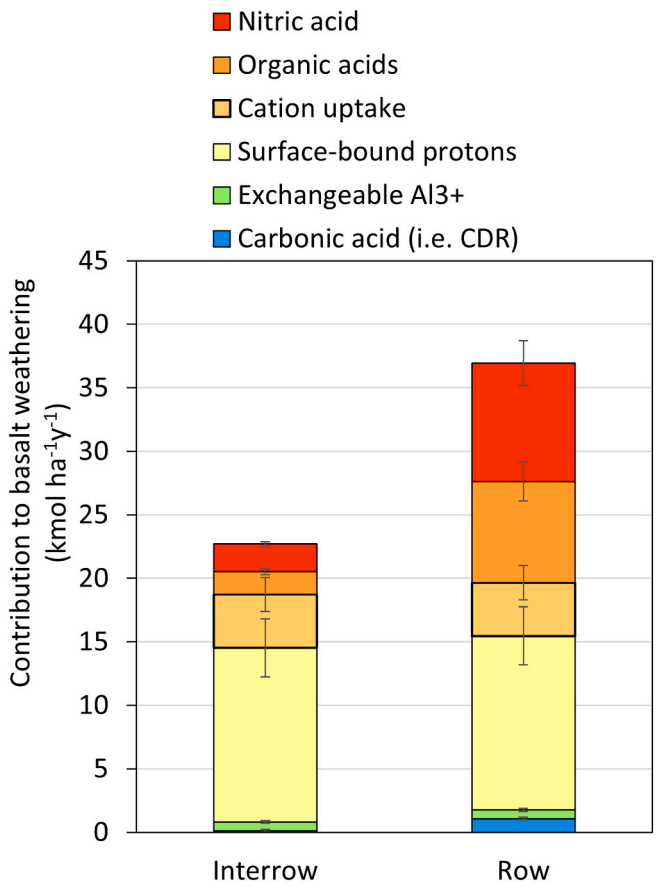

Fig. 3. Contribution of acid sources to weathering of the applied basalt in the row and interrow. While the contribution of most acids to weathering was measured directly, the contribution of organic acids is uncertain as it assumes they were exuded as acids rather than anions. Values derived from soil and plant analyses are the same in the row and interrow, as combined soil samples were used and plant yields were calculated across the whole plot area. Error bars show standard error of the mean.

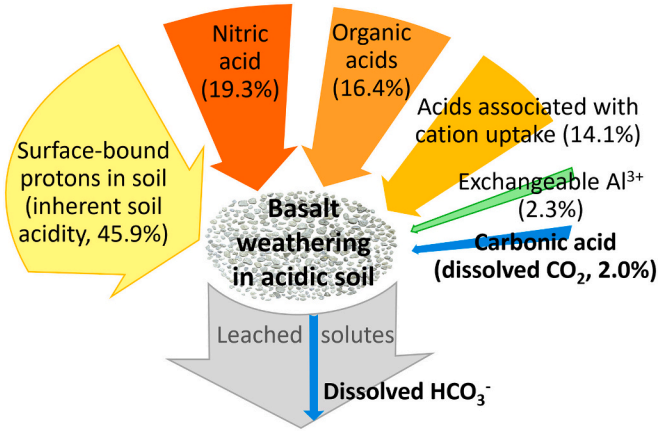

Fig. 4. Relative contribution of acids to weathering of basalt in the field trial over the 2022–2023 year.

moist soil at the study site is conducive to nitrification rather than denitrification, which is alkalising (Weil and Brady, 2017). The importance of nitrogen transformations for solute composition was further indicated by pH fluctuating most in the row, where fertiliser was applied. The typical temporal pattern of leachate pH in the row, starting high then falling rapidly (Fig. 2), was presumably due to initial hydrolysis of urea (an alkalising reaction) followed by nitrification (an acidifying reaction), with more moderate values being attained later in the wet season when most of the fertiliser-derived nitrogen had been taken up or lost (Dong et al., 2022). Urea generally hydrolyses within days (Yadav et al., 1987) although it has been detected in surface runoff from sugarcane fields weeks after application (Davis et al., 2016). Although soil N_2O emissions were not measured in this study, they are likely to have been decreased by basalt application due to its alkalising effect (Blanc-Betes et al., 2021; Chiaravalloti et al., 2023; Hénault et al., 2019).

Plant growth accelerates rock grain weathering, and this effect was apparent in the difference in weathering between the row and interrow (Fig. 3). Five mechanisms are involved: exudation, respiration, decomposition of litter, evapotranspiration, and physical stabilisation (Hinsinger, 2013). Diverse organic acids and siderophores exuded by plants and soil microorganisms enhance weathering; they are produced to increase nutrient uptake as well as mitigate aluminium toxicity and other environmental stressors (Adeleke et al., 2017; Hartmann et al., 2013; Hinsinger, 2013). Significant exudation of oxalic, malic, citric, fumaric and succinic acids has been detected in sugarcane roots (Krishnapriya et al., 2022). Organic acids appear to have contributed substantially to weathering of basalt in this experiment, although their contribution may have been over-estimated because the method assumes they were exuded in protonated form. Plant uptake of cations from solution accelerates weathering (Hartmann et al., 2013; Hinsinger, 2013), but the effect was relatively small here, because cation uptake was only slightly higher in basalt-treated than untreated plots.

4.3. Co-benefits of basalt application

Increased crop yield is a potential co-benefit of EW (Beerling et al., 2018; Hartmann et al., 2013; Swoboda et al., 2022). Sugarcane yield responses to basalt of 9.2–23.6 % over the crop cycle have been achieved in the past with very high basalt application rates of 219–221 t ha^{-1}, similar to the cumulative rate in our trial, but using much finer material (de Villiers, 1961). However, we found no significant effect on yield during the first 5 years of our trial. This suggests sugarcane yields were not limited by supply of the nutrients released by weathering of basalt nor by low pH. Of the likely nutrients, concentrations of Ca, Mg, K and Fe in leaves in the untreated plots at harvest time were all higher than the critical level for sugarcane for leaf 3 during the active growing period (Reuter et al., 1997). Leaf P concentration was lower than the critical level, but soil extractable P was much higher than the critical soil level for sugarcane (Moody and Bolland, 1999) due to a history of overapplication of P fertiliser, suggesting that another factor was limiting P uptake and yield. Leaf N, S and Cu were all low (Reuter et al., 1997) so availability of those elements, as well as low pH, may have limited P uptake.

In the trials reported by de Villiers (1961), yield in the unamended plots was likely limited by nutrients such as Mg and Si, which would have been released by weathering of basalt in the amended plots, as N, P and K fertilisers were applied across the trial. That likelihood is reinforced by the “extremely impoverished” nature of the soils, the “mediocre responses to liberal doses of NPK fertilisers” in the absence of basalt application, and the significantly improved response to NPK fertilisers when basalt was applied. The soil at one site was described as “totally leached out, acid residuum composed mainly of hydrous oxides of iron, aluminium and titanium, with comparatively very little silica”. Furthermore, much finer crushed basalt (described as powder and dust) appears to have been used in the earlier trial, which would have led to faster weathering and nutrient release. It is difficult to speculate further about reasons for the discrepancy between yield response in our trial compared to those reported by de Villiers (1961), as neither basalt mineralogy nor soil and crop nutrient status were reported for those trials. Substantial responses of sugarcane cane and sugar yield to finely ground (Ca,Mg) silicate have also been obtained (Crusciol et al., 2014).

4.4. Implications and conclusions

The results of direct measurements of in-field CDR following basalt application in this trial correspond with modelling studies indicating EW will be less efficient for CDR when applied in acidic conditions (Bertagni and Porporato, 2022; Dietzen and Rosing, 2023; Green et al., 2024; Hartmann et al., 2013). The modelling of basalt weathering in soil by Green et al. (2024) showed very low CDR in acidic conditions (low pH and high pH buffering capacity), despite high weathering rates and cation release, across a range of pCO_2 and other factors. Acidic soils are widespread in regions with a climate conducive to weathering (Hartmann et al., 2013; Sumner and Noble, 2003; Wieder et al., 2014; Zhao et al., 2019), so our results have wider implications. Increased in-field CDR could be expected over time; as soil pH increases due to basalt weathering, and as the alkalisation extends deeper in the soil profile, the contribution of carbonic acid to weathering (Eq. (1)) will increase and the contribution of inherent soil acidity (Eqs. (2) and (3)) will decrease. However, the time and amount of basalt required is uncertain; in our case 250 t ha^{-1} of commercially available crushed basalt over 5 years increased soil pH by only 0.5 units at 0–0.1 m depth, and less than that at deeper depths. Soil pH would need to be raised to a suitable value throughout the regolith, to allow carbonic acid weathering and to prevent HCO_3^- leached from shallower depths being converted to CO_2 (Eq. (3), Fig. 5). Thus, EW appears unlikely to provide cost-effective CDR in strongly acidic soils, and the co-benefits in well-managed commercial sugarcane in this case were also negligible.

Nevertheless, the introduction of crushed basalt into acidic soils, and consequent reaction with strong acids, could be expected to result in net global CDR (assuming low emissions from mining, crushing, transport and spreading) due to (i) reduced emission of CO_2 from soil due to avoided liming (Eq. (4)), (ii) reduced production of CO_2 by acidification of subsoil horizons if they contain carbonate, and (iii) reduced evasion from rivers downstream (Eq. (3), Duvert et al., 2019; Raymond et al., 2013). The leaching of acid at 1.25 m depth was not significantly reduced in this trial (Table 3) but an effect might occur with time. To enable monitoring, reporting and verification (MRV) of global CDR and calculate the economics, the challenge will be to determine the locations and time scales over which CDR occurs across the soil-to-sea continuum, as both will be influenced by ground/surface water hydrology, along with other soil, regolith and catchment characteristics (Zhang et al., 2022). Additional challenges for process modelling that have not yet been fully addressed include (i) spatiotemporal variations in the content (including distribution across pore sizes) and flux of water in the vadose zone, as well as generation of CO_2, acids and alkalis, (ii) variable charge, which plays an important role in acid-base reactions in tropical soils, and (iii) other factors affecting kinetics such as the role of carbonic anhydrase in modulating rates of CDR (Jones et al., 2021; Xiao et al., 2015).

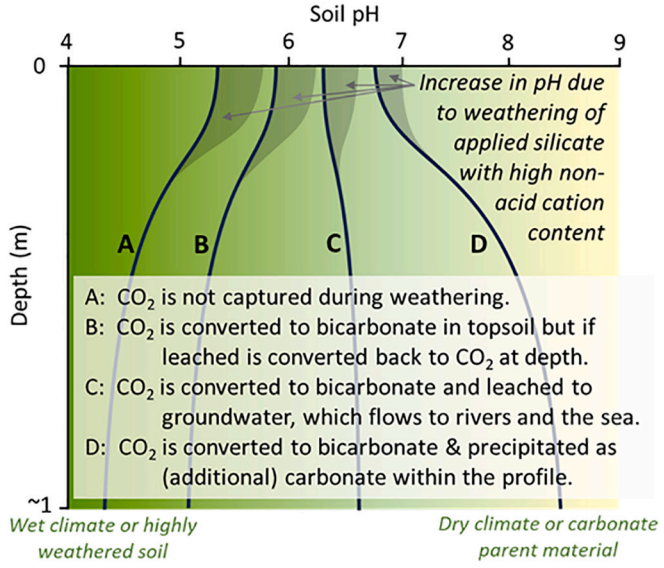

Fig. 5. Hypothetical generalised effects of soil acidity and alkalinity on carbon dioxide capture via enhanced weathering, and the fate of the inorganic carbon generated, shown in 4 scenarios (A, B, C, D), based on the results of this study and the cited literature. Carbon dioxide is captured in scenarios C and D but not in scenarios A or B. The extent to which soil pH and the amount of carbon dioxide captured increase in response to basalt addition (of a given mineralogy, particle size, application rate and incorporation depth) depends not only on soil pH, but also on soil pH buffering capacity and the net acid addition rate of the system, which is related to climate, crop type and management, especially fertilisers. Note that the change in pH for a given addition of alkali (i.e. pH buffer capacity), is fairly constant for a particular soil over the topsoil pH range shown, but the rate of weathering decreases as acidity decreases.

To facilitate CDR via EW within acidic soils, pH could be raised to the range in which carbonic acid weathering is significant, either slowly by applying non-acid-cation-rich silicates, or rapidly by conventional liming with $CaCO_3$ or $(Ca,Mg)CO_3$ (dolomite). At soil pH values too acidic for carbonic acid weathering, silicate weathering will have no effect on CO_2 emission (Eq. (2)), whereas carbonate weathering will generate one mole of CO_2 per mole of carbonate (Hamilton et al., 2007; West and McBride, 2005) via the equation:

$$CaCO_3 + 2HA \rightarrow CO_2\uparrow + Ca^{2+} + 2A^- + H_2O \quad (4)$$

Although the emission of CO_2 is undesirable, lime application will raise pH much more quickly than silicate application.

It is worth comparing silicate and carbonate weathering further. When soil pH is in the range conducive to carbonic acid weathering, weathering of silicates and carbonates are comparable in terms of the stoichiometrically derived index R_{CO2} (mass of CO_2 removed per mass of amendment). Basalts generally have R_{CO2} in the range 0.2–0.4 (Lewis et al., 2021) and that of the Tichum basalt used here was 0.31. Forsterite (Mg_2SiO_4), the end member of the olivine solid-solution series, has one of the highest R_{CO2} of silicates, 1.25. Weathering of carbonates by carbonic acid,

$$CaCO_3 + H_2CO_3 \rightarrow Ca^{2+} + 2HCO_3^- \quad (5)$$

results in half the amount of CDR per mole of non-acid cation charge as weathering of silicates by carbonic acid (Eq. (1)), but the non-acid cation content of carbonates is higher than silicates, so their R_{CO2} is similar; limestone has an R_{CO2} of 0.44. Importantly though, carbonates weather more rapidly than silicates, by 4 orders of magnitude or more (Hartmann et al., 2013), so they are likely to be more effective than silicates for CDR via EW at a soil pH around 6, as well as being more effective for maintaining pH in the optimum range for plants and CDR. Carbonate weathering is integral to global carbon cycling (Gaillardet et al., 1999) and several authors have suggested application of carbonates for CDR via EW (Knapp and Tipper, 2022; Zeng et al., 2022).

One approach for maximising rapid CDR via EW in agricultural soils might involve applying frequent (e.g. annual) applications of limestone or a non-acid-cation-rich silicate to maintain soil pH around 6.4, while minimising application of acidifying inputs such as ammonium fertilisers and maximising pCO_2 by maximising net primary production, root growth and residue retention. Such an approach, with appropriate mechanisms to drive adoption, would optimise benefits for production and other ecosystem services, i.e. sustainable and regenerative agriculture (Nelson, 2023). Regular liming is common practice across humid agricultural zones globally, but it is usually only carried out every several years once pH has dropped substantially. This current practice results in CO_2 emission as well as capture, and uncertainty about the net balance has led to the conservative assumption of the Tier 1 IPCC methodology, that every mole of $CaCO_3$ applied results in one mole of CO_2 emitted (Hamilton et al., 2007; Klein et al., 2006; Page et al., 2009).

However, the overall effect of liming agricultural soils on the global greenhouse gas balance is likely neutral, and liming has a large positive effect on food production (Wang et al., 2021). The carbon balance and life cycle assessment of applying silicates versus lime are yet to be compared, but larger quantities of crushed silicate are needed to raise soil pH by a given amount. It would also be worthwhile conducting more field trials with non-acid-cation-rich silicates in soils with a native pH more likely to be conducive to CDR, i.e. having topsoil pH around 6.4 and a subsoil and regolith with higher pH (Fig. 5). Such soils normally occur in drier climates, but may be irrigated, which would enhance weathering rate and pCO_2.

Irrespective of the amount or type of mineral applied, CDR via EW will be enhanced by reducing application of acidifying inputs (Hartmann et al., 2013). This will be effective not only for in-field CDR but also for avoided evasion downstream. However, a major limitation for any approach aiming to minimise soil acidity and acidifying processes is that the whole regolith must be considered, and prevention or reversal of subsoil acidity is difficult, slow and may not be feasible (Butterly et al., 2022).

In summary, directly measured in-field CDR via EW of crushed basalt (<5 mm) applied over 5 years was small in this tropical sugarcane production system on acidic soil. Most of the basalt weathering (inferred from changes in soil and leachate chemistry) appeared to be due to inherent soil acidity (surface-bound protons) and the concurrent generation of nitric acid (from nitrification), organic acids, and other root exudates, none of which led to in-field CDR (Figs. 4 and 5). These field trial results indicate that in strongly acidic soils EW will be ineffective for CDR, and MRV methods based on weathering rates (such as cation release) will overestimate in-field CDR, confirming conclusions derived from geochemical modelling (Green et al., 2024) and pot trials (Hasemer et al., 2024). Over time, consumption of strong acids via weathering might be expected to result in net CDR more widely due to avoided emission from within the regolith and evasion downstream, as a result of overall higher pH in these locations. Basalt application did not significantly increase crop yield or the stock of carbon in biomass or soil organic matter over the 5-year timeframe, presumably because the nutrients supplied by weathering were not limiting for plant growth, and insufficient secondary minerals were produced to retard decomposition. Further measurements and modelling to quantify CDR via EW in soils across a range of acidity/alkalinity profiles and at the catchment scale are needed, including study of the interactions between soil acidity and weathering of alternative alkaline amendments. Results of this field study will be useful for guiding that research and designing, parameterising, calibrating and validating process-based EW models.

CRediT authorship contribution statement

Fredrick J. Holden: Writing – review & editing, Writing – original draft, Visualization, Methodology, Investigation, Formal analysis, Data curation. **Kalu Davies:** Writing – review & editing, Methodology, Investigation. **Michael I. Bird:** Writing – review & editing, Supervision, Investigation, Conceptualization. **Ruby Hume:** Writing – review & editing, Methodology, Investigation, Formal analysis. **Hannah Green:** Writing – review & editing, Visualization, Methodology, Formal analysis. **David J. Beerling:** Writing – review & editing, Project administration, Funding acquisition, Conceptualization. **Paul N. Nelson:** Writing – review & editing, Writing – original draft, Visualization, Supervision, Project administration, Methodology, Investigation, Formal analysis, Conceptualization.

Declaration of competing interest

The authors declare that the research was conducted in the absence of any commercial or financial relationships that could be construed as a potential conflict of interest. D.J.B. has a minority equity stake in Future Forest/UNDO, is a member of the Advisory Board of The Carbon Community, a UK carbon removal charity, and the Scientific Advisory Council of the non-profit Carbon Technology Research Foundation. P.N. N., F.J.H., M.I.B. and H.G. receive funding for EW research from UNDO Carbon, Consolidated Pastoral Company and Sugar Research Australia.

Acknowledgements

We are grateful to Richard Hesp and his family for allowing us to use their farm and for assisting with the research. Stuart Biggs, Allegra Beaumont, Cécile Bessou, Allison Bryde, Rainy Comley, Dylan Forbes, Jasmine Graham, Hayden Hesp, Viladmir Kaul, Joshua Kelly, Benjamin Krause, Anthony McGann, Hannah Nelson, Rebecca Newman, Olga Odrzygóźdź, Ryan Orr, Ana Palmer, Nikita Tahir, Shannon Todd, Damon Toft and Luke Windle provided help in the field and laboratory, Will Edwards and Tobin Northfield gave statistical advice, Peter van Straaten provided some of the XRF analyses and Amy McBride provided the SEM images. The work was funded by the Leverhulme Trust through the Leverhulme Centre for Climate Change Mitigation (RC-2016-29). F.H. received additional support from the TNQ Drought Hub.

Appendix A. Supplementary data

Supplementary data to this article can be found online at https://doi.org/10.1016/j.scitotenv.2024.176568.

Data availability

Data will be made available on request.

References

Adeleke, R., Nwangburuka, C., Oboirien, B., 2017. Origins, roles and fate of organic acids in soils: A review. S. Afr. J. Bot. 108, 393–406.
Baek, S.H., Kanzaki, Y., Lora, J.M., Planavsky, N., Reinhard, C.T., Zhang, S., 2023. Impact of climate on the global capacity for enhanced rock weathering on croplands. Earth's Future 11 (8), e2023EF003698.
Beerling, D.J., Leake, J.R., Long, S.P., Scholes, J.D., Ton, J., Nelson, P.N., et al., 2018. Farming with crops and rocks to address global climate, food and soil security. Nat. Plants 4 (3), 138–147.
Beerling, D.J., Kantzas, E.P., Lomas, M.R., Wade, P., Eufrasio, R.M., Renforth, P., et al., 2020. Potential for large-scale CO_2 removal via enhanced rock weathering with croplands. Nature 583 (7815), 242–248.
Beerling, D.J., Epihov, D.Z., Kantola, I.B., Masters, M.D., Reershemius, T., Planavsky, N. J., et al., 2024. Enhanced weathering in the US Corn Belt delivers carbon removal with agronomic benefits. PNAS 121, e2319436121.
Berner, R.A., Lasaga, A.C., Garrels, R.M., 1983. The carbonate-silicate geochemical cycle and its effect on atmospheric carbon dioxide over the past 100 million years. Am. J. Sci. (1880) 283 (7), 641–683.
Bertagni, M.B., Porporato, A., 2022. The carbon-capture efficiency of natural water alkalinization: implications for enhanced weathering. Sci. Total Environ. 838, 156524.
Blanc-Betes, E., Kantola, I.B., Gomez-Casanovas, N., Hartman, M.D., Parton, W.J., Lewis, A.L., et al., 2021. In silico assessment of the potential of basalt amendments to reduce N2O emissions from bioenergy crops. GCB Bioenergy 13 (1), 224–241.
Bolan, N.S., Hedley, M.J., 2003. Role of carbon, nitrogen and sulfur cycles in soil acidification. In: Rengel, Z. (Ed.), Handbook of Soil Acidity. Marcel Dekker, New York, U.S.A., pp. 29–56
Brooks, M.E., Kristensen, K., van Benthem, K.J., Magnusson, A., Berg, C.W., Nielsen, A., Skaug, H.J., Maechler, M., Bolker, B.M., 2017. glmmTMB balances speed and flexibility among packages for zero-inflated generalized linear mixed modeling. R J. 9 (2), 378–400.
Bruce, R., Bell, L., Edwards, D., Warrell, L., 1989. Chemical attributes of some Queensland acid soils. II. Relationships between soil and soil solution phase compositions. *Soil Research* 27 (2), 353–364.
Buss, W., Hasemer, H., Ferguson, S., Borevitz, J., 2023. Stabilisation of soil organic matter with rock dust partially counteracted by plants. Glob. Chang. Biol. 30 (1), e17052.
Butterly, C.R., Amado, T.J.C., Tang, C., 2022. Soil acidity and acidification. In: de Oliveira, T.S., Bell, R.W. (Eds.), Subsoil Constraints for Crop Production. Springer Nature Switzerland, Cham, Switzerland, pp. 53–81.
Calabrese, S., Wild, B., Bertagni, M.B., Bourg, I.C., White, C., Aburto, F., et al., 2022. Nano- to global-scale uncertainties in terrestrial enhanced weathering. Environ. Sci. Technol. 56, 15261–15272.
Calcino, D., Schroeder, B., Panitz, J., Hurney, A., Skocaj, D., Wood, A., Salter, B., 2018. Australian Sugarcane Nutrition Manual. Sugar Research Australia, Brisbane.
Chaney, R.L., 2019. Phytoextraction and phytomining of soil nickel. In: Tsadilas, C.D., Rinklebe, J., Selim, H.M. (Eds.), Nickel in Soils and Plants. CRC Press, pp. 341–373.

Chiaravalloti, I., Theunissen, N., Zhang, S., Wang, J., Sun, F., Ahmed, A.A., Pihlap, E., Reinhard, C.T., Planavsky, N.J., 2023. Mitigation of soil nitrous oxide emissions during maize production with basalt amendments. Front. Clim. 5.
Cipolla, G., Calabrese, S., Porporato, A., Noto, L.V., 2022. Effects of precipitation seasonality, irrigation, vegetation cycle and soil type on enhanced weathering–modeling of cropland case studies across four sites. Biogeosciences 19 (16), 3877–3896.
Crusciol, C.A.C., Foltran, R., Rossato, O.B., McCray, J.M., Rossetto, R., 2014. Effects of surface application of calcium-magnesium silicate and gypsum on soil fertility and sugarcane yield. Rev. Bras. Ciênc. Solo 38, 1843–1854.
Crusciol, C.A.C., Soratto, R.P., Gilabel, A.P., Costa, C.H.M.d., Campos, M.D., Castro, G.S. A., Neto, J.F., 2022. Broadcast application of ground silicate rocks as potassium sources for grain crops. Pesq. Agrop. Brasileira 57, e02443.
Davis, A.M., Tink, M., Rohde, K., Brodie, J.E., 2016. Urea contributions to dissolved 'organic' nitrogen losses from intensive, fertilised agriculture. Agric. Ecosyst. Environ. 223, 190–196.
Dessert, C., Dupré, B., Gaillardet, J., François, L.M., Allègre, C.J., 2003. Basalt weathering laws and the impact of basalt weathering on the global carbon cycle. Chem. Geol. 202, 257–273.
Dietzen, C., Rosing, M.T., 2023. Quantification of CO2 uptake by enhanced weathering of silicate minerals applied to acidic soils. Int. J. Greenhouse Gas Control 125, 103872.
Dong, Y., Yang, J.-L., Zhao, X.-R., Yang, S.-H., Mulder, J., Dörsch, P., Zhang, G.-L., 2022. Seasonal dynamics of soil pH and N transformation as affected by N fertilization in subtropical China: an in situ 15N labeling study. Sci. Total Environ. 816, 151596.
Dupla, X., Moeller, B., Baveye, P.C., Grand, S., 2023. Potential accumulation of toxic trace elements in soils during enhanced rock weathering. Eur. J. Soil Sci. 74, e13343.
Duvert, C., Bossa, M., Tyler, K.J., Wynn, J.G., Munksgaard, N.C., Bird, M.I., et al., 2019. Groundwater-derived DIC and carbonate buffering enhance fluvial CO_2 evasion in two Australian tropical rivers. J. Geophys. Res. Biogeosci. 124, 312–327.
Edwards, D.P., Lim, F., James, R.H., Pearce, C.R., Scholes, J., Freckleton, R.P., Beerling, D.J., 2017. Climate change mitigation: potential benefits and pitfalls of enhanced rock weathering in tropical agriculture. Biol. Lett. 13, 20160715.
Gaillardet, J., Dupré, B., Louvat, P., Allegre, C., 1999. Global silicate weathering and CO_2 consumption rates deduced from the chemistry of large rivers. Chem. Geol. 159 (1–4), 3–30.
Gasser, T., Guivarch, C., Tachiiri, K., Jones, C.D., Ciais, P., 2015. Negative emissions physically needed to keep global warming below 2°C. Nat. Commun. 6, 958.
Gee, G.W., Newman, B.D., Green, S.R., Meissner, R., Rupp, H., Zhang, Z.F., et al., 2009. Passive wick fluxmeters: design considerations and field applications. Water Resour. Res. 45, W04420.
Gillman, G., Bell, L., 1978. Soil solution studies on weathered soils from tropical North Queensland. Soil Res. 16 (1), 67–77.
Gillman, G.P., Burkett, D.C., Coventry, R.J., 2002. Amending highly weathered soils with finely ground basalt rock. Appl. Geochemistry 17, 987–1001.
Gillman, G.P., Murtha, G.G., 1983. Effects of sample handling on some chemical properties of soils from high rainfall coastal North Queensland. Aust. J. Soil Res. 21, 67–72.
Goll, D.S., Ciais, P., Amann, T., Buermann, W., Chang, J., Eker, S., et al., 2021. Potential CO_2 removal from enhanced weathering by ecosystem responses to powdered rock. Nat. Geosci. 14, 545–549.
Green, H., Larsen, P., Liu, Y., Nelson, P.N., 2024. Carbon dioxide removal via weathering of sugarcane mill ash under different soil conditions. Appl. Geochem. 165, 105940.
Hamilton, S.K., Kurzman, A.L., Arango, C., Jin, L., Robertson, G.P., 2007. Evidence for carbon sequestration by agricultural liming. Glob. Biogeochem. Cycles 21.
Haque, F., Santos, R.M., Chiang, Y.W., 2020. CO_2 sequestration by wollastonite-amended agricultural soils – an Ontario field study. Int. J. Greenhouse Gas Control 97.
Hartig, F. (2022). DHARMa: residual diagnostics for hierarchical (multi-level / mixed) regression models. R package version 0.4.6, <https://CRAN.R-project.org/package=DHARMa>.
Hartmann, J., West, A.J., Renforth, P., Köhler, P., De La Rocha, C.L., Wolf-Gladrow, D.A., et al., 2013. Enhanced chemical weathering as a geoengineering strategy to reduce atmospheric carbon dioxide, supply nutrients, and mitigate ocean acidification. Rev. Geophys. 51 (2), 113–149.
Hasemer, H., Borevitz, J., Buss, W., 2024. Measuring enhanced weathering: inorganic carbon-based approaches may be required to complement cation-based approaches. Front. Clim. 6, 1352825.
Hénault, C., Bourennane, H., Ayzac, A., Ratié, C., Saby, N., Cohan, J.-P., et al., 2019. Management of soil pH promotes nitrous oxide reduction and thus mitigates soil emissions of this greenhouse gas. Sci. Rep. 9 (1), 1–11.
Hinsinger, P., 2013. Plant-induced changes in soil processes and properties. In: Gregory, P.J., Nortcliff, S. (Eds.), Soil Conditions and Plant Growth. Blackwell Publishing Ltd, pp. 323–365.
Jones, S.P., Kaisermann, A., Ogée, J., Wohl, S., Cheesman, A.W., Cernusak, L.A., Wingate, L., 2021. Oxygen isotope exchange between water and carbon dioxide in soils is controlled by pH, nitrate and microbial biomass through links to carbonic anhydrase activity. SOIL 7, 145–159.
Kantola, I.B., Blanc-Betes, E., Masters, M.D., Chang, E., Marklein, A., Moore, C.E., Haden, A., Bernacchi, C.J., Wolf, A., Epihov, D.Z., Beerling, D.J., DeLucia, E.H., 2023. Improved net carbon budgets in the US Midwest through direct measured impacts of enhanced weathering. Glob. Chang. Biol. 29 (24), 7012–7028.
Kantzas, E.P., Val Martin, M., Lomas, M.R., Eufrasio, R.M., Renforth, P., Lewis, A.L., Taylor, L.L., Mecure, J.-F., Pollitt, H., Vercoulen, P.V., Vakilifard, N., Holden, P.B., Edwards, N.R., Koh, L., Pidgeon, N.F., Banwart, S.A., Beerling, D.J., 2022. Substantial carbon drawdown potential from enhanced rock weathering in the United Kingdom. Nat. Geosci. 15 (5), 382–389.
Klein, C. D., Novoa, R., Ogle, S., Smith, K., Rochette, P., Wirth, T., … Rypdal, K. (2006). Chapter 11: N2O emissions from managed soils, and CO2 emissions from lime and urea application. In 2006 IPCC Guidelines for National Greenhouse Gas Inventories. Volume 4: Agriculture, Forestry and Other Land Use (Vol. Technical Report 4-88788-032-4): Intergovernmental Panel on Climate Change.
Klemme, A., Rixen, T., Müller, M., Notholt, J., Warneke, T., 2022. Destabilization of carbon in tropical peatlands by enhanced weathering. Commun. Earth Environ. 3 (1), 212.
Knapp, W.J., Tipper, E.T., 2022. The efficacy of enhancing carbonate weathering for carbon dioxide sequestration. Front. Clim. 4, 928215.
Köhler, P., Hartmann, J., Wolf-Gladrow, D.A., 2010. Geoengineering potential of artificially enhanced silicate weathering of olivine. Proc. Natl. Acad. Sci. 107 (47), 20228–20233.
Krishnapriya, V., Karpagam, E., Arun Kumar, R., Gomathi, R., Chandran, K., Vasantha, S., Alagupalamuthirsolai, M., 2022. Genotypic diversity in the type and quantum of root exudates in Saccharum complex and allied genera. J. Sugarcane Res. 12 (2), 172–185.
Larkin, C.S., Andrews, M.G., Pearce, C.R., Yeong, K.L., Beerling, D.J., Bellamy, J., et al., 2022. Quantification of CO_2 removal in a large-scale enhanced weathering field trial on an oil palm plantation in Sabah. Malaysia. Front. Clim. 4, 959229.
Lefebvre, D., Goglio, P., Williams, A., Manning, D.A., de Azevedo, A.C., Bergmann, M., et al., 2019. Assessing the potential of soil carbonation and enhanced weathering through life cycle assessment: A case study for Sao Paulo state, Brazil. J. Clean. Prod. 233, 468–481.
Lewis, A.L., Sarkar, B., Wade, P., Kemp, S.J., Hodson, M.E., Taylor, L.L., et al., 2021. Effects of mineralogy, chemistry and physical properties of basalts on carbon capture potential and plant-nutrient element release via enhanced weathering. Appl. Geochem. 105023.
Linke, T., Oelkers, E., Diderikesen, K., Möckel, S., Nilabh, S., Grandia, F., Gislason, S., 2024. The geochemical evolution of basalt enhanced rock weathering systems quantified from a natural analogue. Geochim. Cosmochim. Acta 370, 66–77.
Low, S., Baum, C.M., Sovacool, B.K., 2022. Taking it outside: exploring social opposition to 21 early-stage experiments in radical climate interventions. Energy Res. Soc. Sci. 90, 102594.
Markewitz, D., Davidson, E.A., Figueiredo, R. de O., Victoria, R.L., Krusche, A.V., 2001. Control of cation concentrations in stream waters by surface soil processes in an Amazonian watershed. Nature 410 (6830), 802–805.
Moody, P.W., Bolland, M.D.A., 1999. Phosphorus. In: Peverill, K.I., Sparrow, L.A., Reuter, D.J. (Eds.), Soil Analysis: An Interpretation Manual. CSIRO Publishing, Collingwood, pp. 187–220.
Murtha, G. G., Cannon, M. G., & Smith, C. D. (1996). Soils of the Babinda-Cairns Area, North Queensland. Division of Soils Divisional Report No. 123: CSIRO Division of Soils.
Nelson, P., Su, N., 2010. Soil pH buffering capacity: a descriptive function and its application to some acidic tropical soils. Aust. J. Soil Res. 48 (3), 201–207.
Nelson, P. N. (2023). Sustainable soil management in tropical agriculture. In Somasundaram Jayaraman, R. C. Dalal, & R. Lal (Eds.), Sustainable Soil Management: Beyond Food Production (pp. 204–239). Newcastle upon Tyne: Cambridge Scholars Publishing.
Page, K.L., Allen, D.E., Dalal, R.C., Slattery, W., 2009. Processes and magnitude of CO_2, CH_4, and N_2O fluxes from liming of Australian acidic soils: a review. Aust. J. Soil Res. 47 (8), 747–762.
Posit team, 2024. RStudio: Integrated Development Environment for R. Posit Software, PBC, Boston, MA. http://www.posit.co/.
R Core Team, 2024. R: A Language and Environment for Statistical Computing. R Foundation for Statistical Computing, Vienna, Austria. https://www.R-project.org/>.
Rayment, G.E., Lyons, D.J., 2011. Soil Chemical Methods: Australasia. CSIRO Publishing, Collingwood.
Raymond, P.A., Hartmann, J., Lauerwald, R., Sobek, S., McDonald, C., Hoover, M., et al., 2013. Global carbon dioxide emissions from inland waters. Nature 503 (7476), 355–359.
Reuter, D.J., Edwards, D.G., Wilhelm, N.S., 1997. Temperate and tropical crops. In: Reuter, D.J., Robinson, J.B. (Eds.), Plant Analysis: An Interpretation Manual. CSIRO Publishing, Collingwood, Australia, pp. 83–284.
Reershemius, T., Nelson, P.N., Davies, K., Bird, M.I., Kalderon-Asael, B., Asael, D., Epihov, D.Z., Beerling, D.J., Reinhard, C.T., Planavsky, N.J., 2023. Quantifying carbon dioxide removal in an enhanced rock weathering field trial in Queensland, Australia: a soil-based mass balance approach. Presentation at the Goldschmidt 2023 Conference (unpublished results).
Riahi, K., Schaeffer, R., Arango, J., Calvin, K., Guivarch, C., Hasegawa, T., … Vuuren, D. P. v. (2022). Mitigation pathways compatible with long-term goals. . In P. R. Shukla, J. Skea, R. Slade, A. A. Khourdajie, R. v. Diemen, D. McCollum, M. Pathak, S. Some, P. Vyas, R. Fradera, M. Belkacemi, A. Hasija, G. Lisboa, S. Luz, & J. Malley (Eds.), *IPCC, 2022: Climate Change 2022: Mitigation of Climate Change. Contribution of Working Group III to the Sixth Assessment Report of the Intergovernmental Panel on Climate Change*. Cambridge, UK and New York, USA: Cambridge University Press.
Robinson, N., Brackin, R., Vinall, K., Soper, F., Holst, J., Gamage, H., et al., 2011. Nitrate paradigm does not hold up for sugarcane. PLoS One 6 (4), e19045.
Rosentreter, J.A., Eyre, B.D., 2019. Alkalinity and dissolved inorganic carbon exports from tropical and subtropical river catchments discharging to the great barrier reef, Australia. Hydrol. Process. 2020, 1530–1544.
Schuiling, R., Krijgsman, P., 2006. Enhanced weathering: an effective and cheap tool to sequester CO2. Clim. Chang. 74 (1), 349–354.
Sherrod, L.A., Dunn, G., Peterson, G.A., Kolberg, R.L., 2002. Inorganic carbon analysis by modified pressure-calcimeter method. Soil Sci. Soc. Am. J. 66 (1), 299–305.

Soil Survey Staff, 2022. Keys to Soil Taxonomy, 13th ed. USDA-Natural Resources Conservation Service, Washington DC.
Sokol, N.W., Sohng, J., Moreland, K., Slessarev, E., Goertzen, H., Schmidt, R., Samaddar, S., Holzer, I., Almaraz, M., Geoghegan, E., 2024. Reduced accrual of mineral-associated organic matter after two years of enhanced rock weathering in cropland soils, though no net losses of soil organic carbon. Biogeochemistry 167, 989–1005.
van Straaten, P., 2006. Farming with rocks and minerals: challenges and opportunities. An. Acad. Bras. Cienc. (Ann. Braz. Acad. Sci.) 78 (4), 731–747.
Strefler, J., Amann, T., Bauer, N., Kriegler, E., Hartmann, J., 2018. Potential and costs of carbon dioxide removal by enhanced weathering of rocks. Environ. Res. Lett. 13.
Sumner, M.E., Noble, A.D., 2003. Soil acidification: The world story. In: Rengel, Z. (Ed.), Handbook of Soil Acidity. Marcel Dekker, New York, U.S.A., pp. 1–28
Swoboda, P., Döring, T.F., Hamer, M., 2022. Remineralizing soils? The agricultural usage of silicate rock powders: A review. Sci. Total Environ. 807, 150976.
Taylor, L.L., Quirk, J., Thorley, R.M.S., Kharecha, P.A., Hansen, J., Ridgwell, A., et al., 2016. Enhanced weathering strategies for stabilizing climate and averting ocean acidification. Nat. Clim. Chang. 6, 402–408.
Taylor, L.L., Driscoll, C.T., Groffman, P.M., Rau, G.H., Blum, J.D., Beerling, D.J., 2021. Increased carbon capture by a silicate-treated forested watershed affected by acid deposition. Biogeosciences 18 (1), 169–188.
Van Breemen, N., Mulder, J., Driscoll, C.T., 1983. Acidification and alkalinization of soils. Plant Soil 75, 283–308.
de Villiers, O.d'H., 1961. Soil rejuvenation with crushed basalt in Mauritius. Part I: consistent results of worldwide interest. Int. Sugar J. 63, 363–364.
Wang, X., Tang, C., Mahony, S., Baldock, J.A., Butterly, C.R., 2015. Factors affecting the measurement of soil pH buffer capacity: approaches to optimize the methods. Eur. J. Soil Sci. 66, 53–64.
Wang, X., Tang, C., Mahony, S., Baldock, J.A., Butterly, C.R., 2017. Corrigendum. Eur. J. Soil Sci. 68, 793.
Wang, Y., Yao, Z., Zhan, Y., Zheng, X., Zhou, M., Yan, G., Wang, L., Werner, C., Butterbach-Bahl, K., 2021. Potential benefits of liming to acid soils on climate change mitigation and food security. Glob. Chang. Biol. 27 (12), 2807–2821.
Weil, R.R., Brady, N.C., 2017. The Nature and Properties of Soils, 15th Edition ed. Pearson, Upper Saddle River, New Jersey, USA.
West, T.O., McBride, A.C., 2005. The contribution of agricultural lime to carbon dioxide emissions in the United States: dissolution, transport, and net emissions. Agric. Ecosyst. Environ. 108, 145–154.
Whitehead, P.W., Stephenson, P.J., McDougall, I., Hopkins, M.S., Grahams, A.W., Collerson, K.D., Johnson, D.P., 2007. Temporal development of the Atherton Basalt Province, North Queensland. Aust. J. Earth Sci. 54 (5), 691–709.
Wieder, W.R., Boehnert, J., Bonan, G.B., & Langseth, M. (2014). Regridded Harmonized World Soil Database v1.2. Data set. Available on-line [http://daac.ornl.gov] from Oak Ridge National Laboratory Distributed Active Archive Center, Oak Ridge, Tennessee, USA.
Wood, S.N., 2011. Fast stable restricted maximum likelihood and marginal likelihood estimation of semiparametric generalized linear models. J. R. Stat. Soc. Ser. B 73 (1), 3–36.
Xiao, L., Lian, B., Hao, J., Liu, C., Wang, S., 2015. Effect of carbonic anhydrase on silicate weathering and carbonate formation at present day CO_2 concentrations compared to primordial values. Sci. Rep. 5, 7733.
Xu, T., Yuan, Z., Vicca, S., Goll, D.S., Li, G., Lin, L., Chen, H., Bi, B., Chen, Q., Li, C., Wang, X., Wang, C., Hao, Z., Fang, Y., Beerling, D.J., 2024. Enhanced silicate weathering accelerates forest carbon sequestration by stimulating the soil mineral carbon pump. Glob. Chang. Biol. 30 (8), e17464.
Yadav, D., Kumar, V., Singh, M., Relan, P., 1987. Effect of temperature and moisture on kinetics of urea hydrolysis and nitrification. Soil Res. 25 (2), 185–191.
Zeng, S., Liu, Z., Groves, C., 2022. Large-scale CO_2 removal by enhanced carbonate weathering from changes in land-use practices. Earth Sci. Rev. 225, 103915.
Zhang, S., Planavsky, N.J., Katchinoff, J., Raymond, P.A., Kanzaki, Y., Reershemius, T., Reinhard, C.T., 2022. River chemistry constraints on the carbon capture potential of surficial enhanced rock weathering. Limnol. Oceanogr. 67, S148–S157.
Zhao, X., Yang, Y., Shen, H., Geng, X., Fang, J., 2019. Global soil–climate–biome diagram: linking surface soil properties to climate and biota. Biogeosciences 16, 2857–2871.